Short Strings in Three-Dimensional Anti–de Sitter Space: From Weak to Strong Coupling

Simon Ekhammar,[1,2,*] Nikolay Gromov,[1,†] Bogdan Stefański, Jr.,[3,‡] and Charles Thull[3,§]
[1]*Department of Mathematics, King's College London, Strand WC2R 2LS, London, United Kingdom*
[2]*Department of Physics and Astronomy, Uppsala University, Box 516, SE-751 20 Uppsala, Sweden*
[3]*Centre for Mathematics Innovation, City St George's, University of London, Northampton Square, EC1V 0HB, London, United Kingdom*

(Received 1 April 2026; accepted 26 May 2026; published 25 June 2026)

We numerically solve the conjectured quantum spectral curve for strings on $\mathrm{AdS}_3 \times \mathrm{S}^3 \times \mathrm{T}^4$ with Ramond-Ramond charge from weak to strong coupling. At strong coupling, the spectrum organizes into flat-space string mass levels with universal square-root scaling in the string tension at leading order, and additional Kaluza-Klein fine-splitting at subleading order. At weak coupling, the energies are determined by a nearest-neighbor Bethe *Ansatz*, with universal subleading corrections that are suppressed at large volume.

DOI: 10.1103/3kxd-wjvs

Introduction—The AdS/CFT correspondence [1] is an exact duality relating free strings on anti–de Sitter (AdS) space to planar conformal field theory (CFT). In principle, solving string theory in AdS provides nonperturbative access to strongly coupled CFTs. However, first-principle quantization of Ramond-Neveu-Schwarz strings in many anti–de Sitter backgrounds remains an outstanding problem, since Ramond-Ramond (R–R) vertex operators introduce nonlocal world-sheet interactions. Remarkably, in certain highly symmetric backgrounds, Green-Schwarz string theory is integrable [2], suggesting that the full spectrum can be encoded into a set of integrability-based equations. This hope has been realized in $\mathrm{AdS}_5 \times \mathrm{S}^5$ and $\mathrm{AdS}_4 \times \mathbb{CP}^3$ through the quantum spectral curve (QSC) formalism [3,4].

Inspired by this higher-dimensional success, a QSC for free strings on $\mathrm{AdS}_3 \times \mathrm{S}^3 \times \mathrm{T}^4$ supported by pure RR charges was conjectured in [5,6]. Compared to its higher-dimensional cousins, this model presents many additional conceptual and technical challenges [7,8]. In this Letter, we overcome these difficulties to find nontrivial solutions of the QSC numerically and, for the first time, predict the AdS_3 string spectrum from weak to strong coupling—a goal that has driven the integrability programme since its inception more than 15 years ago [9]. Our results, summarized in Fig. 1, show the conformal dimensions of low-lying operators throughout the full coupling range in terms of $\lambda_h \equiv 16\pi^2 h^2$, with h the integrability coupling constant [10]. While in the present Letter we focus on an $\mathfrak{sl}(2)$ sector of operators, we expect that our methods can be extended to probe the full operator spectrum.

AdS$_3$ and holography: Strings on $\mathrm{AdS}_3 \times \mathrm{S}^3 \times \mathrm{T}^4$ occupy a distinguished place in holography. Through the AdS/CFT correspondence, they are expected to describe the near-horizon D1–D5 system [1], which has played a central role in microscopic black-hole entropy counting. Moreover, two-dimensional CFTs are much more constrained than their higher-dimensional counterparts, raising

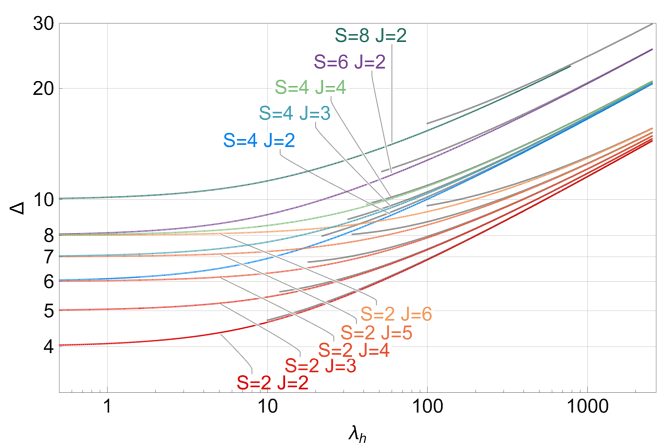

FIG. 1. The numerical QSC spectrum for a wide range of couplings, $\lambda_h \equiv 16\pi^2 h^2$, and for different states labeled by their spin, S, and R-charge, J. A stringy spectrum emerges at strong coupling, with energy levels in agreement with flat-space string theory together with additional KK modes for the two lowest mass levels. The gray lines show the strong coupling prediction (15).

*Contact author: simon.ekhammar@kcl.ac.uk
†Contact author: nikolay.gromov@kcl.ac.uk
‡Contact author: bogdan.stefanski.1@citystgeorges.ac.uk
§Contact author: charles.thull@citystgeorges.ac.uk

the prospect of a particularly sharp realization of holography. At the same time, AdS_3 backgrounds exhibit features absent in higher dimensions, including long strings, continuous spectra, and a multidimensional moduli space acted on by a large U-duality group, making them a fertile testing ground for holographic ideas; see, for example, Refs. [11–15].

For AdS_3 backgrounds supported purely by Neveu-Schwarz-Neveu-Schwarz flux, the string spectrum can be determined using Wess-Zumino-Witten methods [14]. Additionally, at minimal Neveu-Schwarz-Neveu-Schwarz flux the hybrid formalism [16] yields an exact match with the symmetric-orbifold CFT [17–19]. However, away from these special loci, the duality is expected to exhibit significantly richer dynamics, especially along continuous 't Hooft-like coupling directions that are believed to realize weak-strong holography, as in higher-dimensional AdS/CFT examples. Progress in this regime therefore hinges on the availability of genuinely quantitative methods, such as the QSC framework.

Weak coupling and the CFT regime: At weak coupling $h \ll 1$, the anomalous dimensions for our QSC solutions Δ satisfy

$$\Delta = \Delta_0 + h^2\Delta_1 + \mathcal{O}(h^3), \tag{1}$$

with $\Delta_0 \in \mathbb{Z}_{>0}$. The leading corrections Δ_1 coincide with the spectrum of an integrable nearest-neighbour $\mathfrak{sl}_2$ spin chain, in agreement with the structure for the weakly coupled planar description of the CFT proposed in [20]. Our results extend previous analytical calculations [7] to operators with larger charges and uncover novel wrapping corrections at $\mathcal{O}(h^3)$, providing the first controlled access to finite-size effects at weak coupling. These findings offer concrete spectral CFT data in a region of moduli space far removed from the symmetric-orbifold point.

A stringy spectrum: At strong coupling $\lambda_h \gg 1$, the integrability coupling is expected to be related to the inverse string tension, α', as $\sqrt{\lambda_h} \simeq R^2_{\mathrm{AdS}}/\alpha'$, with R_{AdS} the radius of AdS_3; cf. Ref. [21]. This relation suggests that the strong-coupling regime may be viewed as a flat-space limit, in which the spectrum should organize itself into Regge trajectories labeled by mass levels $\Delta^2 \sim 4\delta/\alpha' \simeq 4\sqrt{\lambda_h}\delta$ for positive integer δ (in $R_{\mathrm{AdS}} = 1$ unit), where δ counts the total string oscillator excitations' level. The compact S^3 introduces Kaluza-Klein (KK) modes, splitting each Regge trajectory at subleading order in λ_h into a tower of states with different spherical angular momenta.

The QSC is a symmetry-based construction following from $\mathfrak{psu}(1,1|2)^{\oplus 2}$ representation theory and analyticity constraints, and, *a priori*, it is not obvious that it knows about string theory. Still, our solutions reveal the emergence of Regge trajectories, KK towers, and the characteristic $\lambda_h^{1/4}$ scaling expected for strings on $AdS_3 \times S^3 \times T^4$. Our numerical results, summarized in Fig. 1, reveal precisely this structure at strong coupling, with states clustering into string levels characterized by

$$\Delta = 2\sqrt{\delta}\lambda_h^{\frac{1}{4}} + E_0 + E_1\lambda_h^{-\frac{1}{4}} + E_2\lambda_h^{-\frac{2}{4}} + \mathcal{O}\left(\lambda_h^{-\frac{3}{4}}\right), \tag{2}$$

where all E_n coefficients, except E_0, which we found to be 0, depend on the angular momentum in S^3. This provides strong support for the conjecture [5,6] that the QSC captures the quantum spectrum of free strings in this background.

In what follows, we present the numerical methods underlying these results and make quantitative comparisons with semiclassical strings at strong coupling and the asymptotic Bethe *Ansatz* (ABA) at weak coupling. The QSC provides for the first time access to the full coupling range, furnishing concrete spectral data for precision holography in AdS_3.

The AdS_3 *quantum spectral curve*—The starting point for the QSC is the superalgebra $\mathfrak{psu}(1,1|2)^{\oplus 2}$, reflecting the left-right symmetry of a nonchiral two-dimensional CFT and generating the superisometries of $AdS_3 \times S^3$. We distinguish the right-moving copy by using dotted indices. This algebra has two spacetime charges, the conformal dimension Δ and the spin S, as well as two R-symmetry charges J and K. The role of the QSC is to lift this classical symmetry algebra to a quantum deformation.

This is achieved through a supersymmetric Q system [22–24], which promotes relations amongst characters to Hirota-like finite difference equations. The Q system comprises functions of a spectral parameter u whose large-u asymptotics encode the global charges, while their analytic structure—controlled by the coupling h—encodes the infinite tower of integrable charges. Each $\mathfrak{psu}(1,1|2)$ Q system contains four distinguished Q functions, $\mathbf{P}_a$, $\mathbf{Q}_k$ with a, $k = 1$, 2, from which all other Q functions can be constructed. We recall the complete structure in Appendix A in the End Matter.

The quantum deformation is specified by demanding polynomial asymptotics,

$$\mathbf{P}_a \sim u^{M_a}, \quad \mathbf{Q}_k \sim u^{\hat{M}_k}, \quad \mathbf{P}_{\dot{a}} \sim u^{M_{\dot{a}}}, \quad \mathbf{Q}_{\dot{k}} \sim u^{\hat{M}_{\dot{k}}}, \tag{3}$$

where $M, \hat{M}$ are linear combinations of the classical charges Δ, S, J, K [5]. Higher integrable charges are encoded in $1/u$ corrections to these asymptotics. However, the lift from classical to quantum algebra is not unique—different analytic properties yield different integrable models. For $AdS_3 \times S^3 \times T^4$, the analytic structure was conjectured in [5,6]: the P functions have a short branch cut on $[-2h, 2h]$, introducing the coupling h, while the Q functions possess an infinite tower of cuts spaced by i extending into the lower half-plane from the real axis. The two Q systems are then related by gluing along $[-2h, 2h]$,

$$\mathbf{Q}_k(u + i0) = G_k{}^{\dot{p}}\bar{\mathbf{Q}}_{\dot{p}}(u - i0), \quad G = \begin{pmatrix} 0 & i\alpha \\ -i/\alpha & 0 \end{pmatrix}, \tag{4}$$

where α is a real function of the coupling and $\bar{\mathbf{Q}}_l$ denotes complex conjugation. These analytic properties, together with the algebraic Q-system relations, fully quantize the model and determine its spectrum.

In this Letter we focus on solutions with quantum numbers $\Delta|_{h=0} = J + S$ and $K = 0$ and parity symmetry $u \leftrightarrow -u$. The subset of these states with $J = 2$ was previously studied at weak coupling in [7].

QSC at weak coupling: We begin in the weak-coupling regime, where the QSC can be solved analytically and its analytic structure can be elucidated. This will inform the subsequent numerical analysis at strong coupling.

The key technical feature distinguishing AdS_3 from higher-dimensional cases is that the branch points at $\pm 2h$ are logarithmic rather than quadratic [25], reflecting the presence of gapless world-sheet modes. This necessitates a double-sum *Ansatz* [7],

$$\mathbf{P}_a = \sum_{k=0}^{\infty} \sum_{m=0}^{k} h^k l^m \mathbf{P}_a^{(k,m)}, \tag{5}$$

where $l = (i/2\pi)\log[(x-1)/(x+1)]$ and $\mathbf{P}_a^{(k,m)}$ are Laurent polynomials in the Zhukovsky variable,

$$x(u) = \frac{1}{2h}\left(u + \sqrt{u^2 - 4h^2}\right). \tag{6}$$

Solving the Q-system relations subject to the gluing condition (4) and extracting dimensions from large-u asymptotics, we extend previous $J = 2$ results [7] to the full $J = 3$ sector (computed for $S = 2, \ldots, 12$, but expected to hold for general S),

$$\begin{aligned}\Delta(J=3,S) = {} & J + S + 8\mathbf{S}_1 h^2 + \frac{512}{63\pi}\mathbf{S}_1^2 h^3 \\ & + \left(\gamma_{\mathcal{N}=4}^{(4),J=3} - \frac{8192}{525\pi^2}\mathbf{S}_1^3\right) h^4 + \mathcal{O}(h^5),\end{aligned} \tag{7}$$

with harmonic sums $\mathbf{S}_k = \sum_{n=1}^{S/2} n^{-k}$ and $\gamma_{\mathcal{N}=4}^{(4),J=3} = -8\mathbf{S}_3 - 4\mathbf{S}_1\mathbf{S}_2$ [26]. For $J = 2$, we recover the result of [7] and verify its validity at larger values of S.

At $\mathcal{O}(h^2)$, these results reproduce the AdS_3 ABA and match the corresponding $\mathcal{N} = 4$ supersymmetric Yang-Mills (SYM) dimensions. Intriguingly, for both $J = 2, 3$ all terms computed match $\mathcal{N} = 4$ SYM in the formal limit $1/\pi \to 0$ [7]. The $\mathcal{O}(h^3)$ term is absent in the ABA, and as argued below, is suppressed as $J \to \infty$; we would thus interpret it as a wrapping correction. Remarkably, the coefficient γ_3 of h^3 is proportional to $(\gamma_2)^2$ (where γ_2 is the h^2 coefficient) with an S-independent rational prefactor. Combining these analytic results for arbitrary S with numerical fits (as described below) at $S = 2, J = 4, 5, \ldots, 8$ and $S = 4, J = 4$, we find a universal expression,

$$\gamma_3 = \frac{2(J+1)}{(2J+1)(2J+3)\pi}(\gamma_2)^2, \tag{8}$$

which we conjecture to hold for general J and S. The existence of such an unexpected relation suggests that there may be a modified ABA capable of capturing small-h corrections rather than large-volume effects, analogous to the $\mathcal{N} = 4$ case [27]. Such a formulation would provide analytical weak-coupling starting points essential for systematic numerical studies and warrants future investigation.

Numerical approach—To reach finite and strong coupling, numerical methods are essential, since no exact analytic expression $\Delta(h)$ in terms of elementary functions is likely to exist, as evidenced by the nontrivial weak coupling expansion. In AdS_5 and AdS_4, where branch cuts are quadratic, one parametrizes the $\mathbf{P}$ functions as

$$\mathbf{P}_a \simeq x^{M_a} \sum_{k=0}^{\text{cutoff}} \frac{c_{a,k}}{x^{2k}}, \tag{9}$$

where the x^{-2k} basis exploits parity symmetry. The Zhukovsky variable x resolves the quadratic branch cut singularity, yielding exponential convergence even at $|x| = 1$ (i.e., on the cut in u). However, in AdS_3 the logarithmic branch-cut structure means x no longer removes the branch points. For example, the logarithm l from (5) expands as $l \propto \sum_{k\,\text{odd}} (kx^k)^{-1}$, exhibiting only power-law convergence $\sim 1/k$. This severely limits the numerical efficiency of this basis.

Standard convergence acceleration addresses this by using basis functions that resum such slowly converging series. Motivated by the logarithmic structure in (5), we introduce the polylogarithm combinations

$$L_n(x) = \sum_{k=1}^{n} a_{k,n} \mathrm{Li}_k(x^{-2}) = x^{-2n} + \mathcal{O}(x^{-2n-2}), \tag{10}$$

where the right-hand side implicitly defines the coefficients $a_{k,n}$. With the modified *Ansatz*

$$\mathbf{P}_a = x^{M_a} \sum_{k=0}^{\text{cutoff}} c_{a,k} L_k(x), \tag{11}$$

we achieve dramatically improved performance, reaching reliable results up to $h \sim 4$ ($\lambda_h \sim 2500$), a substantial improvement over the $h < 0.1$ limit of previous methods [7], which we reproduce in the overlap region.

The numerical algorithm: With the *Ansatz* (11), we solve the QSC following [28]. We first solve the Q-system relations and then evaluate the gluing condition (4) on the cut $[-2h, 2h]$. For a set of sampling points $I \subset [-2h, 2h]$, we minimize the cost function,

$$F(\{c_{a,n}, c_{\dot{a},n}\}, \Delta) = \sum_{u \in I} \left| \mathbf{Q}_k(u + i0) - G_k{}^{l} \bar{\mathbf{Q}}_l(u - i0) \right|^2, \tag{12}$$

which vanishes for exact solutions. We use a Newton-type method to optimize the coefficients $c_{a,n}$, $c_{\dot{a},n}$, the dimension Δ, and the gluing matrix parameter α.

A key refinement is the choice of sampling points I. Rather than the standard Chebyshev nodes, we concentrate points near the ends of branch cuts $\pm 2h$ via $u_i = 2h\,\mathrm{sign}(t_i)[1-(1-|t_i|)^\beta]$, where $\{t_i\}$ are roots of the Chebyshev polynomial $T_n(t)$ and $\beta = 5/3$. This choice provides good numerical stability and improves the resolution of the singular behavior where the gluing condition is most sensitive.

The numerical solution of the QSC in the sector of states considered in this Letter is simplified by the availability of weak-coupling analytic and numerical results [7]. These provide good initial values for the Newton-type methods we use here. Extending our analysis to more general sectors of states will likewise require corresponding weak-coupling data to initialize the algorithm.

The spectrum at strong coupling—We study two series of states (Fig. 1): $(J=2, S=2,4,6,8)$ and the KK tower $(S=2, J=2,\ldots,8)$, as well as states with $S=4, J=3$, 4. Our numerical results are presented in Tables 1 and II in Appendix D.

Fitting our numerical data to a series in $\lambda_h^{-1/4}$, we find excellent agreement with (2) for $\delta = S/2$ and $E_0 = 0$. This is highly nontrivial: different QSCs exhibit distinct strong-coupling asymptotics, and the QSC construction itself contains, *a priori*, no string theory input. Moreover, we find $E_2 \neq 0$, a novel feature absent in higher-dimensional examples.

To extract subleading coefficients, we use the fitting procedure of [29], where following $\mathcal{N}=4$ SYM, we assume terms $\lambda_h^{-a/2}$ with $a>1$ are absent. Our results strongly suggest that, up to an overall $1/\sqrt{S}$ factor, the $\lambda_h^{-1/4}$ coefficient depends only on J^2, S, S^2. Assuming this structure, we find, with an uncertainty in last digit,

$$4\sqrt{2S}\Delta|_{\lambda_h^{-1/4}} = 2.00000J^2 - 3.9995S + 2.9998S^2. \qquad (13)$$

The $\lambda_h^{-1/2}$ term is simpler, scaling linearly with J,

$$\Delta|_{\lambda_h^{-1/2}} = 0.50002J. \qquad (14)$$

These numerical values strongly suggest integer coefficients, as in higher dimensions. We therefore conjecture the exact expansion,

$$\Delta = \sqrt{2S}\lambda_h^{1/4} + \frac{2J^2 - 4S + 3S^2}{4\lambda_h^{1/4}\sqrt{2S}} + \frac{J}{2\lambda_h^{1/2}} + \ldots. \qquad (15)$$

This resembles the $AdS_5 \times S^5$ short string spectrum, with the key novelty being the $\lambda_h^{-1/2}$ term. Figure 1 shows excellent visual agreement between (15) and our numerical data.

The AdS Virasoro-Shapiro amplitude [30] was recently extended to AdS_3 [31–33], leading to results up to $\mathcal{O}(\lambda^{-1/4})$ for related but distinct states (see Appendix C). They find an expression similar to (15), differing only by $-4S \to -2S$ in the $\lambda^{-1/4}$ coefficient. Since the states differ, no direct comparison is possible; moreover, the coefficient can be shifted by a state-independent reparametrization $\lambda_h(\lambda)$. The next-order term at $\lambda_h^{-3/4}$, which we provide below, will be essential for a meaningful comparison with independent approaches.

Extracting the $\lambda_h^{-3/4}$ coefficient is considerably more challenging, as numerical precision degrades rapidly for subleading terms. Motivated by $\mathcal{N}=4$ SYM, where states on the same conformal Regge trajectory as a Bogomol'nyi–Prasad–Sommerfield operator exhibit a particular structure, we assume that the coefficient takes the form $(2S)^{-3/2}$ times a linear combination of $J^4, J^2S, J^2S^2, S^2, S^3, S^4$ [34]. We emphasize that this is an assumption that requires future justification—it is known to fail for generic states in $\mathcal{N}=4$ SYM, which contain nonpolynomial dependence on charges due to mixing [35]. Fitting all our states (excluding $S=8$, for which we have not reached $h=4$), we find

$$32(2S)^{3/2}\Delta|_{\lambda_h^{-3/4}} = -3.9991J^4 + 19.9S^2J^2 - 15.8SJ^2 - 21.0006S^4 - 1.98S^3 - 23.5S^2. \qquad (16)$$

Some coefficients appear reliably integer, while others do not. We therefore propose

$$\Delta|_{\lambda_h^{-3/4}} = \frac{20J^2S^2 - 4J^4 - 21S^4 + c_1J^2S + c_2S^2 + c_3S^3}{32(2S)^{3/2}}, \qquad (17)$$

leaving c_1, c_2, c_3 undetermined. Our data suggest that c_1 and c_3 may also be integers. If one further assumes that any deviation from integer values arises from transcendental terms proportional to ζ_3, as occurs in $\mathcal{N}=4$, the best fit yields (with some uncertainty)

$$c_1 \simeq -16, \qquad c_2 \simeq -2, \qquad c_3 \simeq 92 - 96\zeta_3. \qquad (18)$$

Extending the Virasoro-Shapiro calculations of [31–33] to this order would provide valuable insight into which coefficients are integers and which contain transcendental numbers.

Classical string comparison: Beyond comparing to flat-space string expectations, we can test our results against classical strings in curved AdS space. We compare against the folded string solution [36,37], which is the lowest-energy classical configuration with the same quantum numbers and parity symmetry as our states. While a classical solution describes a macroscopic string with charges scaling as $S, J \sim \sqrt{\lambda_h}$, we can reexpand the classical expression [34] to compare with our short-string results,

$$\Delta_{\mathrm{cl}} = \sqrt{2S}\lambda_h^{\frac{1}{4}} + \frac{2J^2+3S^2}{4\sqrt{2S}\lambda_h^{1/4}} - \frac{4J^4-20J^2S^2+21S^4}{32(2S)^{3/2}\lambda_h^{3/4}} + \ldots . \quad (19)$$

This yields perfect agreement with the terms with maximal powers of S and J at $\lambda_h^{1/4}, \lambda_h^{-1/4}$ in (15) and $\lambda_h^{-3/4}$ in (17). This provides yet another nontrivial confirmation that the QSC captures quantum string dynamics in AdS. The lower order terms from (15) and (17) absent in (19) represent quantum corrections to the classical energy. In particular, the $\lambda_h^{-1/2}$ term should be captured by a one-loop calculation. It would be interesting to revisit previous results [38–40] in light of our findings.

Conclusions and outlook—We have found nontrivial solutions of the conjectured RR $\mathrm{AdS}_3 \times \mathrm{S}^3 \times \mathrm{T}^4$ QSC from weak to strong coupling, determining for the first time the spectrum of classes of short strings across a large coupling range. Our findings reveal a rich structure bridging integrable spin-chain physics at weak coupling and stringy Regge trajectories at strong coupling.

At weak coupling, the spectrum starts from a nearest-neighbor $\mathfrak{sl}_2$ integrable spin chain [20], mirroring $\mathcal{N} = 4$ SYM and Aharony-Bergman-Jafferis-Maldacena theory. Novel features emerge at higher orders: odd powers of the coupling reminiscent of Balitsky-Fadin-Kuraev-Lipatov physics [41], and inverse powers of π suggestive of infrared effects from massless modes. Understanding their precise origin—for instance, as infrared bubble effects within the perturbative framework of [20]—may illuminate a new formulation of the CFT near the weakly coupled RR point in moduli space.

At strong coupling, short strings organize into flat-space Regge trajectories splitting into S^3 KK towers. Remarkably, this stringy structure emerges from a purely symmetry-based construction, providing strong evidence for the QSC conjecture [5,6]. While not observed in the states explored from the AdS_3 Virasoro-Shapiro amplitude [33], the non-vanishing $\lambda_h^{-1/2}$ corrections are consistent with infrared dynamics of massless modes [42,43]. We leave the detailed exploration of these terms, for example through semi-classical string analysis, to future work.

Our methods open several compelling directions. States with massless excitations are accessible with modified analytic properties and h^1 scaling, which it would be interesting to compare with related results obtained using the thermodynamic Bethe *Ansatz* [45,46]. Adapting our approach to states studied via Virasoro-Shapiro amplitudes [31–33] (see Appendix C) would provide a direct test of the QSC. Similarly, adapting our methods to the computation of the Hagedorn temperature will allow comparison against effective string theory results, successful in higher dimensions to several subleading orders [47–49]. Mixed-flux backgrounds [50–52], where the $h \to 0$ limit should reproduce [21] the Wess-Zumino-Witten spectrum [14], offer another important setting; cf. the recent proposal for thermodynamic Bethe *Ansatz* equations [53]. Finally, extending our numerical approach to $\mathrm{AdS}_3 \times \mathrm{S}^3 \times \mathrm{S}^3 \times \mathrm{S}^1$ [9,54–56] is a further interesting direction.

Acknowledgments—We are grateful to A. Cavaglià, F. Chernikov, P. Ryan, A Torrielli, and D. Volin for collaboration on related topics as well as to B. Basso, S. Chester, S. Frolov, A. Georgoudis, D. Polvara, A. Sfondrini, A. Tseytlin, and D.-l. Zhong for fruitful discussions. The work of S. E. was conducted with funding awarded by the Swedish Research Council, Vetenskapsrådet, Grant No. VR 2024-00598. The work of N. G. was supported by the European Research Council (ERC) under the European Union's Horizon 2020 research and innovation program—60—(Grant Agreement No. 865075) EXACTC. B. S. and C. T. acknowledge funding support from an STFC Consolidated Grant "Theoretical Particle Physics at City, University of London" ST/T000716/1 and ST/X000729/1. The work of N. G. was supported by the Science Technology and Facilities Council under the Grants No. ST/P000258/1 and No. ST/X000753/1.

Data availability—The data that support the findings of this article are openly available in Appendix D of this article.

[1] J. M. Maldacena, Adv. Theor. Math. Phys. **2**, 231 (1998).
[2] I. Bena, J. Polchinski, and R. Roiban, Phys. Rev. D **69**, 046002 (2004).
[3] N. Gromov, V. Kazakov, S. Leurent, and D. Volin, Phys. Rev. Lett. **112**, 011602 (2014).
[4] A. Cavaglià, D. Fioravanti, N. Gromov, and R. Tateo, Phys. Rev. Lett. **113**, 021601 (2014).
[5] A. Cavaglià, N. Gromov, B. Stefański, Jr., and A. Torrielli, J. High Energy Phys. 12 (2021) 048.
[6] S. Ekhammar and D. Volin, J. High Energy Phys. 03 (2022) 192.
[7] A. Cavaglià, S. Ekhammar, N. Gromov, and P. Ryan, J. High Energy Phys. 12 (2023) 089.
[8] S. Ekhammar, N. Gromov, and B. Stefański, J. High Energy Phys. 10 (2025) 188.
[9] A. Babichenko, B. Stefanski, Jr., and K. Zarembo, J. High Energy Phys. 03 (2010) 058.
[10] The zero-coupling values Δ_0 shown as the x intercept, reflect our particular choice of operators and should not be taken as exhaustive. Other values, including half-integer ones, will exist for other operator choices.
[11] A. Giveon, D. Kutasov, and N. Seiberg, Adv. Theor. Math. Phys. **2**, 733 (1998).
[12] N. Seiberg and E. Witten, J. High Energy Phys. 04 (1999) 017.
[13] F. Larsen and E. J. Martinec, J. High Energy Phys. 06 (1999) 019.
[14] J. M. Maldacena and H. Ooguri, J. Math. Phys. (N.Y.) **42**, 2929 (2001).
[15] O. Aharony and E. Y. Urbach, Phys. Rev. D **110**, 046028 (2024).
[16] N. Berkovits, C. Vafa, and E. Witten, J. High Energy Phys. 03 (1999) 018.

[17] M. R. Gaberdiel and R. Gopakumar, J. High Energy Phys. 05 (2018) 085.
[18] L. Eberhardt, M. R. Gaberdiel, and R. Gopakumar, J. High Energy Phys. 04 (2019) 103.
[19] A. Dei, L. Eberhardt, and M. R. Gaberdiel, J. High Energy Phys. 12 (2019) 012.
[20] O. Ohlsson Sax, A. Sfondrini, and B. Stefanski, J. High Energy Phys. 06 (2015) 103.
[21] O. Ohlsson Sax and B. Stefański, J. High Energy Phys. 05 (2018) 101.
[22] V. Kazakov, A. S. Sorin, and A. Zabrodin, Nucl. Phys. **B790**, 345 (2008).
[23] Z. Tsuboi, Nucl. Phys. **B826**, 399 (2010).
[24] V. Kazakov, S. Leurent, and D. Volin, J. High Energy Phys. 12 (2016) 044.
[25] R. Borsato, O. Ohlsson Sax, A. Sfondrini, B. Stefanski, Jr., and A. Torrielli, Phys. Rev. D **88**, 066004 (2013).
[26] A. V. Kotikov, L. N. Lipatov, A. Rej, M. Staudacher, and V. N. Velizhanin, J. Stat. Mech. (2007) P10003.
[27] N. Beisert and M. Staudacher, Nucl. Phys. **B727**, 1 (2005).
[28] N. Gromov, F. Levkovich-Maslyuk, and G. Sizov, J. High Energy Phys. 06 (2016) 036.
[29] N. Gromov, A. Hegedus, J. Julius, and N. Sokolova, J. High Energy Phys. 05 (2024) 185.
[30] L. F. Alday and T. Hansen, J. High Energy Phys. 10 (2023) 023.
[31] S. M. Chester and D.-l. Zhong, Phys. Rev. Lett. **134**, 151602 (2025).
[32] H. Jiang and D.-l. Zhong, J. High Energy Phys. 02 (2026) 071.
[33] H. Jiang, arXiv:2601.18646.
[34] N. Gromov and S. Valatka, J. High Energy Phys. 03 (2012) 058.
[35] S. Ekhammar, N. Gromov, and P. Ryan, J. High Energy Phys. 12 (2024) 165.
[36] S. S. Gubser, I. R. Klebanov, and A. M. Polyakov, Nucl. Phys. **B636**, 99 (2002).
[37] S. Frolov and A. A. Tseytlin, J. High Energy Phys. 06 (2002) 007.
[38] M. Beccaria, F. Levkovich-Maslyuk, G. Macorini, and A. A. Tseytlin, J. High Energy Phys. 04 (2013) 006.
[39] M. Beccaria and G. Macorini, J. High Energy Phys. 03 (2013) 040.
[40] V. Forini, V. G. M. Puletti, and O. Ohlsson Sax, J. Phys. A **46**, 115402 (2013).
[41] S. Ekhammar, N. Gromov, and M. Preti, arXiv:2406.18639.
[42] R. Roiban and A. A. Tseytlin, J. High Energy Phys. 11 (2009) 013.
[43] We note that the presence of terms at this order in the strong-coupling expansion is not entirely without precedent in related contexts; the reader may find it instructive to consult the discussion surrounding Eq. (4.10) of [44], where a careful analysis of the $\mathfrak{su}(1|1)$ sector of $\mathrm{AdS}_5 \times \mathrm{S}^5$ reveals a broadly analogous structure, the precise interpretation of which in that setting is discussed in subsequent sections by the authors.
[44] G. Arutyunov and S. Frolov, J. High Energy Phys. 01 (2006) 055.
[45] S. Frolov and A. Sfondrini, J. High Energy Phys. 03 (2022) 138.
[46] A. Brollo, D. le Plat, and A. Sfondrini, arXiv:2512.15697.
[47] T. Harmark and M. Wilhelm, J. High Energy Phys. 07 (2022) 136.
[48] S. Ekhammar, J. A. Minahan, and C. Thull, J. Phys. A **56**, 435401 (2023).
[49] S. Ekhammar, J. A. Minahan, and C. Thull, J. High Energy Phys. 10 (2023) 066.
[50] B. Hoare and A. A. Tseytlin, Nucl. Phys. **B873**, 682 (2013).
[51] T. Lloyd, O. Ohlsson Sax, A. Sfondrini, and B. Stefański, Jr., Nucl. Phys. **B891**, 570 (2015).
[52] B. Hoare, A. Stepanchuk, and A. A. Tseytlin, Nucl. Phys. **B879**, 318 (2014).
[53] S. Frolov, D. Polvara, and A. Sfondrini, J. High Energy Phys. 02 (2026) 237.
[54] O. Ohlsson Sax and B. Stefanski, Jr., J. High Energy Phys. 08 (2011) 029.
[55] A. Cavaglià, R. Frassek, N. Primi, and R. Tateo, arXiv:2511.09635.
[56] F. Chernikov, S. Ekhammar, N. Gromov, and B. Smith, arXiv:2511.09654.
[57] R. Borsato, O. Ohlsson Sax, A. Sfondrini, B. Stefański, and A. Torrielli, J. High Energy Phys. 08 (2013) 043.

End Matter

Appendix A: A brief reminder of the AdS_3 *QSC*—In this appendix, we recap the general formulas for the AdS_3 QSC and give details on the algorithm for the perturbative solution for the particular states considered in this Letter.

The AdS_3 QSC consists of two $\mathfrak{psu}(1,1|2)$ Q systems connected through analytic continuation. Each Q system consists of 16 Q functions satisfying QQ relations,

$$Q^+_{a|i} - Q^-_{a|i} = \mathbf{P}_a \mathbf{Q}_i, \qquad \mathbf{Q}_i = -\mathbf{P}^a Q^+_{a|i}, \tag{A1}$$

$$Q^+_{\dot{a}|\dot{k}} - Q^-_{\dot{a}|\dot{k}} = \mathbf{P}_{\dot{a}} \mathbf{Q}_{\dot{k}}, \qquad \mathbf{Q}_{\dot{k}} = -\mathbf{P}^{\dot{a}} Q^+_{\dot{a}|\dot{k}}, \tag{A2}$$

where $f^\pm = f[u \pm (i/2)]$. These functions have the asymptotics

$$\mathbf{P}_a \simeq \mathbb{A}_a u^{M_a}, \qquad \mathbf{P}^a \simeq \mathbb{A}^a u^{-M_a - 1},$$
$$\mathbf{Q}_k \simeq \mathbb{B}_k u^{\hat{M}_k}, \qquad \mathbf{Q}^k \simeq \mathbb{B}^k u^{-\hat{M}_k - 1}, \tag{A3}$$

$$M_a = \frac{1}{2}\{-J + K - 2, J - K\} - \frac{\hat{B}}{2},$$
$$\hat{M}_k = \frac{1}{2}\{\Delta - S, -\Delta + S - 2\} + \frac{\hat{B}}{2}, \tag{A4}$$

$$M_{\dot{a}} = \frac{1}{2}\{-J-K, J+K-2\} - \frac{\check{B}}{2}, \qquad \hat{M}_{\dot{k}} = \frac{1}{2}\{\Delta+S-2, -\Delta-S\} + \frac{\check{B}}{2}, \tag{A5}$$

and the leading coefficients $\mathbb{A}_a$ are given as

$$\mathbb{A}_1\mathbb{A}^1 = -\mathbb{A}_2\mathbb{A}^2 = -\frac{i}{4}\frac{(\Delta-J+K-S)(\Delta+J-K-S+2)}{J-K+1}, \tag{A6}$$

$$\mathbb{A}_{\dot{1}}\mathbb{A}^{\dot{1}} = -\mathbb{A}_{\dot{2}}\mathbb{A}^{\dot{2}} = -\frac{i}{4}\frac{(\Delta-J-K+S)(\Delta+J+K+S-2)}{J+K-1}, \tag{A7}$$

$$\mathbb{B}_1\mathbb{B}^1 = -\mathbb{B}_2\mathbb{B}^2 = \frac{i}{4}\frac{(\Delta-J+K-S)(\Delta+J-K-S+2)}{\Delta-S+1}, \tag{A8}$$

$$\mathbb{B}_{\dot{1}}\mathbb{B}^{\dot{1}} = -\mathbb{B}_{\dot{2}}\mathbb{B}^{\dot{2}} = \frac{i}{4}\frac{(\Delta-J-K+S)(\Delta+J+K+S-2)}{\Delta+S-1}. \tag{A9}$$

(Following [7], we changed $S \to -S$ and $K \to -K$ compared to [8].) The $\mathbf{Q}$ functions can be found from the $\mathbf{P}$ functions by solving the Baxter equation,

$$D_1^- \mathbf{Q}_k^{++} - D_2\mathbf{Q}_k + D_1^+\mathbf{Q}_k^{--} = 0, \tag{A10}$$

where

$$D_1 = \epsilon_{ab}(\mathbf{P}^a)^-(\mathbf{P}^b)^+,$$
$$D_2 = \epsilon_{ab}(\mathbf{P}^a)^{--}(\mathbf{P}^b)^{++} - \mathbf{P}_c(\mathbf{P}^c)^{--}\epsilon_{ab}\mathbf{P}^a(\mathbf{P}^b)^{++}.$$

As a boundary condition on the Q system we have the constraint

$$\det(Q_{a|i}) = \det\left(Q_{\dot{a}|\dot{i}}\right) = 1. \tag{A11}$$

On the first Riemann sheet the $\mathbf{P}$ functions have a short branch cut on the interval $[-2h, 2h]$. By consistency, the $\mathbf{Q}$ functions have on the first Riemann sheet an infinite tower of cuts, with the first one on the real line interval $[-2h, 2h]$ and the rest of the tower spaced by i and extending into the lower half plane. The $Q_{a|i}$ functions have a similar tower of cuts but shifted by $-\frac{i}{2}$ into the lower half-plane.

In this Letter, we consider states with $K=0$ and $\Delta(h=0) = J+S$. For these states, we find $\mathbf{P}_a = \epsilon_{ab}\mathbf{P}^b$ and the parity relation

$$\mathbf{P}_a(-u) = \mathbf{g}_a^b\mathbf{P}_b(u), \tag{A12}$$

with $\mathbf{g}_a^b = (-1)^{M_a}\delta_a^b$ and similar for the dotted functions. The analytic continuation of the $\mathbf{P}$ functions through their first branch cut on a path $\bar{\gamma}$ counterclockwise around the point $u=-2h$ can then be written in the form

$$\mathbf{P}_a = \mu_a^{R\dot{b}}(\mathbf{P}_{\dot{b}})^{\bar{\gamma}}. \tag{A13}$$

The matrix μ^R is constructed as

$$\mu_a^{R\dot{b}} = -Q_{a|k}\left(u+\frac{i}{2}\right)\epsilon^{kl}G_l{}^{\dot{m}}e^{-i\pi\hat{M}_{\dot{m}}}Q_{\dot{c}|\dot{m}}\epsilon^{\dot{c}\dot{d}}\mathbf{g}_{\dot{d}}^{\dot{b}}, \tag{A14}$$

in terms of the gluing matrix (4) and it has no branch cuts on the real line. An analogous equation gives $\mu_{\dot{a}}^{Rb}$.

Appendix B: Analytic solutions of the QSC—The QSC can be solved analytically using the coupling h as a small expansion parameter. The algorithm presented here is a refinement of the algorithm developed in [7].

For $J=2$, 3 the tree-level ($h=0$) $\mathbf{P}$ functions are monomials in u. Using this, it is easy to solve the Baxter equation for Q and the QQ relations for $Q_{a|i}$, followed by applying the determinant constraint to fully fix the tree-level solution.

At the QQ scale we make the *Ansatz*

$$\mathbf{P}_a = \mathbb{A}_a u^{M_a}\left(1+\sum_{n=1}^{\infty} c_{a,n}\frac{h^{2n}}{u^{2n}}\right), \tag{B1}$$

with the coefficients expanding as $c_{a,n} = c_{a,n}^{(0)} + \mathcal{O}(h)$. We use this *Ansatz* to solve order by order the QQ relations for the $Q_{a|i}$ and $\mathbf{Q}$ functions. The asymptotics of the $\mathbf{Q}$ functions and the determinant constraint (A11) fix most of the integration constants. Using (A14) we can then construct $\mu^R(u), \dot{\mu}^R(u)$ with the parameter of the gluing matrix expanding as $\alpha = \alpha^{(0)}h^J + \mathcal{O}(h^{J+1})$. Since these μ^R matrices do not have a branch cut on the real line, we can change variables to $v = (u/h)$ and at finite order in h the μ^R are a finite order polynomial in v. Requiring μ^R to be unambiguous, namely the absence of any regularization parameter, provides at this stage some additional constraints on the integration constants. We can then compute the matrix $W_a^c(v) = \mu_a^{R\dot{b}}\mu_{\dot{b}}^{Rc}$, which describes the double analytic continuation of the $\mathbf{P}$ functions,

$$\mathbf{P}_a = W_a^b \mathbf{P}_b^{2\bar{\gamma}}. \tag{B2}$$

By construction W has unit determinant. As the $\mathbf{P}$ functions should be regular near the branch points $u = \pm 2h$, the trace of W is constrained as

$$\mathrm{tr} W(v = \pm 2) = 2 \tag{B3}$$

such that W approaches the identity matrix near the branch points of P.

The final constraint in order to fix the solution of the QSC is the analytic continuation. This cannot be imposed using the *Ansatz* (B1) in the variable u. Instead, we make a second *Ansatz* (5) using the Zhukovsky variable x

$$\mathbf{P}_a = \sum_{k=0}^{\infty} \sum_{m=0}^{k} h^k l^m \mathbf{P}_a^{(k,m)}, \tag{B4}$$

with $l = (i/2\pi) \log [(x-1)/(x+1)]$ and $\mathbf{P}_a^{(k,m)}$ are Laurent polynomials in x of finite degree. Applying the definition of the Zhukovsky variable and expanding the new *Ansatz* at small h we can relate the coefficients in both *Ansätze*. Noting that $v = x + (1/x)$, $x^{\bar{\gamma}} = (1/x)$ and $l^{\bar{\gamma}} = l + \frac{1}{2}$, we finally test the analytic continuation

$$\mathbf{P}_a = \mu_a^{R\dot{b}} (\mathbf{P}_{\dot{b}})^{\bar{\gamma}}. \tag{B5}$$

Following this algorithm to an appropriate order in h, the dimension of the state in consideration is fixed to the desired order.

Appendix C: Comparison with the AdS_3 *Virasoro-Shapiro amplitude*—The states we study differ from those appearing in the Virasoro-Shapiro amplitude approach [31–33]. Following the AdS_3 integrability convention [57], we label multiplets by the highest weight state obtained from the superconformal primary by acting with two right-moving supercharges. Our states have even spin $S \in 2\mathbb{Z}_{>0}$ and equal left and right R-charges $(J/2)$, so the corresponding superconformal primaries have odd spin $S-1$ and R charges $\{(J/2), [(J-2)/2]\}$. The Virasoro-Shapiro amplitude instead exchanges multiplets whose superconformal primaries have spin $l \in 2\mathbb{Z}_{>0}$ and equal left and right R charges $[(p-1)/2]$ $(p \in \mathbb{Z}_{>0})$.

We note in particular that for $J = 2$, the (4,4) superconformal primary is *not* part of the lowest massive string multiplet. In contrast, in $\mathcal{N} = 4$ SYM theory and its string dual, the analogous state (meaning the $\mathcal{N} = 4$ state with all Cartan charges outside $\mathfrak{psu}(1,1|2)^{\oplus 2}$ set to zero) would be a descendant of the Konishi multiplet, obtained by the action of two supercharges. These supercharges, however, are not part the small (4,4) superconformal algebra and are broken in the AdS_3 setting. As a result, the $J = 2$ (4,4) primary we study here sits in a distinct long multiplet within the lowest massive string level, unrelated to the Konishi.

Appendix D: Data—In this appendix, we present our complete numerical results for the anomalous dimensions of operators with charges S and J for a range of couplings h. The numerical uncertainty below in Δ is of order 10^{-10}.

TABLE I. Dimension of operators for various states.

h	Δ	h	Δ	h	Δ	h	Δ	h	Δ	h	Δ	h	Δ
$S=2,\ J=2$													
0.01	4.001207282	0.08	4.078225448	0.6	6.135613947	1.3	8.501275846	2	10.35712566	2.7	11.93117562	3.4	13.32182153
0.02	4.004853461	0.09	4.098743466	0.7	6.521109233	1.4	8.789868414	2.1	10.59615815	2.8	12.13953087	3.5	13.50886858
0.03	4.010963707	0.1	4.121454961	0.8	6.887778530	1.5	9.069517300	2.2	10.82997795	2.9	12.34439471	3.6	13.69337328
0.04	4.019547323	0.2	4.445163873	0.9	7.237562305	1.6	9.340984008	2.3	11.05890840	3	12.54593600	3.7	13.87543619
0.05	4.030597147	0.3	4.865328931	1	7.572295971	1.7	9.604931396	2.4	11.28324113	3.1	12.74431048	3.8	14.05515142
0.06	4.044089416	0.4	5.303718475	1.1	7.893597294	1.8	9.861939847	2.5	11.50324016	3.2	12.93966217	3.9	14.23260721
0.07	4.059984063	0.5	5.729701596	1.2	8.202859617	1.9	10.11252044	2.6	11.71914541	3.3	13.13212453	4	14.40788643
							$S=2,\ J=3$						
0.01	5.000802328	0.08	5.051403636	0.6	6.654157824	1.3	8.840353308	2	10.62588434	2.7	12.16018454	3.4	13.52451905
0.02	5.003216499	0.09	5.064886187	0.7	6.997386434	1.4	9.115576817	2.1	10.85798831	2.8	12.36416158	3.5	13.70848916
0.03	5.007248380	0.1	5.079840990	0.8	7.330203728	1.5	9.383283024	2.2	11.08537760	2.9	12.56488416	3.6	13.89005041
0.04	5.012897096	0.2	5.298979111	0.9	7.652184950	1.6	9.643999153	2.3	11.30831910	3	12.76250067	3.7	14.06929402
0.05	5.020154907	0.3	5.604364921	1	7.963600453	1.7	9.898203972	2.4	11.52705650	3.1	12.95714877	3.8	14.24630568
0.06	5.029007215	0.4	5.948183326	1.1	8.265002365	1.8	10.14633103	2.5	11.74181285	3.2	13.14895642	3.9	14.42116599
0.07	5.039432710	0.5	6.302548717	1.2	8.557035834	1.9	10.38877269	2.6	11.95279280	3.3	13.33804278	4	14.59395083

(Table continued)

TABLE I. *(Continued)*

h	Δ	h	Δ	h	Δ	h	Δ	h	Δ	h	Δ	h	Δ
						$S = 2,\ J = 4$							
0.01	6.000553648	0.08	6.035369982	0.6	7.296462457	1.3	9.284668920	2	10.98447065	2.7	12.46861871	3.4	13.79912532
0.02	6.002217055	0.09	6.044672167	0.7	7.596197143	1.4	9.543901936	2.1	11.20791770	2.8	12.66700092	3.5	13.97910773
0.03	6.004991668	0.1	6.055011825	0.8	7.892673594	1.5	9.797198337	2.2	11.42723992	2.9	12.86241884	3.6	14.15684814
0.04	6.008875888	0.2	6.209863436	0.9	8.183883668	1.6	10.04484383	2.3	11.64264046	3	13.05499670	3.7	14.33242651
0.05	6.013865044	0.3	6.436819010	1	8.468891898	1.7	10.28712374	2.4	11.85430849	3.1	13.24485074	3.8	14.50591827
0.06	6.019951411	0.4	6.706488396	1.1	8.747349799	1.8	10.52431479	2.5	12.06242010	3.2	13.43208983	3.9	14.67739471
0.07	6.027124265	0.5	6.997424134	1.2	9.019228184	1.9	10.75668080	2.6	12.26713925	3.3	13.61681606	4	14.84692319
						$S = 2,\ J = 5$							
0.01	7.000400366	0.08	7.025562770	0.6	8.030782349	1.3	9.820243187	2	11.42470860	2.7	12.85095733	3.4	14.14159254
0.02	7.001602433	0.09	7.032301387	0.7	8.289844066	1.4	10.06206318	2.1	11.63826858	2.8	13.04278945	3.5	14.31683326
0.03	7.003606526	0.1	7.039802553	0.8	8.550953222	1.5	10.29951841	2.2	11.84833655	2.9	13.23198059	3.6	14.49002235
0.04	7.006411457	0.2	7.153783104	0.9	8.811291648	1.6	10.53267532	2.3	12.05505113	3	13.41862927	3.7	14.66122738
0.05	7.010014511	0.3	7.326580176	1	9.069171268	1.7	10.76163949	2.4	12.25854579	3.1	13.60282879	3.8	14.83051250
0.06	7.014411466	0.4	7.539934509	1.1	9.323608373	1.8	10.98653903	2.5	12.45894823	3.2	13.78466748	3.9	14.99793867
0.07	7.019596607	0.5	7.778372386	1.2	9.574056916	1.9	11.20751381	2.6	12.65638018	3.3	13.96422898	4	15.16356384
						$S = 2,\ J = 6$							
0.01	8.000301382	0.08	8.019243955	0.6	8.831959867	1.3	10.43307282	2	11.93775134	2.7	13.30098096	3.4	14.54724543
0.02	8.001205951	0.09	8.024325568	0.7	9.055016989	1.4	10.65706217	2.1	12.14067306	2.8	13.48557685	3.5	14.71715886
0.03	8.002713729	0.1	8.029987823	0.8	9.283677887	1.5	10.87813753	2.2	12.34073697	2.9	13.66786938	3.6	14.88522468
0.04	8.004823913	0.2	8.116857576	0.9	9.514874201	1.6	11.09618439	2.3	12.53802126	3	13.84793159	3.7	15.05149775
0.05	8.007534877	0.3	8.251609095	1	9.746552049	1.7	11.31115569	2.4	12.73260665	3.1	14.02583390	3.8	15.21603059
0.06	8.010844175	0.4	8.422640984	1.1	9.977351693	1.8	11.52305042	2.5	12.92457460	3.2	14.20164405	3.9	15.37887349
0.07	8.014748550	0.5	8.619017595	1.2	10.20638302	1.9	11.73189866	2.6	13.11400614	3.3	14.37542709	4	15.54007461
						$S = 2,\ J = 7$							
0.02	9.000937819	0.04	9.003750964	0.06	9.008433210	0.08	9.014970705	0.1	9.023342168				
0.03	9.002110185	0.05	9.005859138	0.07	9.011471210	0.09	9.018928802						
						$S = 2,\ J = 8$							
0.05	10.00467917	0.06	10.00673536	0.07	10.00916275	0.08	10.01195982	0.09	10.01512472	0.1	10.01865537		

TABLE II. Dimension of operators for various states.

h	Δ	h	Δ	h	Δ	h	Δ	h	Δ	h	Δ	h	Δ
						$S = 4,\ J = 2$							
0.1	6.171427121	0.7	9.535460935	1.3	12.29122301	1.9	14.53884762	2.5	16.48317513	3.1	18.22119771	3.7	19.80726508
0.2	6.630181806	0.8	10.04552155	1.4	12.69338457	2	14.88054761	2.6	16.78534988	3.2	18.49499258	3.8	20.05941816
0.3	7.223132199	0.9	10.53207751	1.5	13.08325462	2.1	15.21458042	2.7	17.08217943	3.3	18.76479199	3.9	20.30844005
0.4	7.838282371	1	10.99779223	1.6	13.46188103	2.2	15.54143851	2.8	17.37393756	3.4	19.03076589	4	20.55444461
0.5	8.433369477	1.1	11.44496598	1.7	13.83017406	2.3	15.86156407	2.9	17.66087551	3.5	19.29307255		
0.6	8.998967873	1.2	11.87555563	1.8	14.18892956	2.4	16.17535591	3	17.94322445	3.6	19.55185961		
						$S = 4,\ J = 3$							
0.1	7.120966473	0.7	9.933697089	1.3	12.55892384	1.9	14.75142637	2.5	16.66404565	3.1	18.38097531	3.7	19.95176975
0.2	7.452503142	0.8	10.41023653	1.4	12.94911533	2	15.08674094	2.6	16.96214856	3.2	18.65190032	3.8	20.20176659
0.3	7.908837693	0.9	10.86990720	1.5	13.32840298	2.1	15.41490513	2.7	17.25515859	3.3	18.91897371	3.9	20.44872289
0.4	8.415492935	1	11.31352115	1.6	13.69759199	2.2	15.73634659	2.8	17.54332493	3.4	19.18235401	4	20.69274641
0.5	8.931925714	1.1	11.74215628	1.7	14.05740467	2.3	16.05145346	2.9	17.82687745	3.5	19.44218924		
0.6	9.440265336	1.2	12.15693336	1.8	14.40848884	2.4	16.36057900	3	18.10602861	3.6	19.69861790		
						$S = 4,\ J = 4$							
0.01	8.000878797	0.08	8.056391594	0.6	9.996709987	1.3	12.91338223	2	15.36351991	2.7	17.48899926	3.4	19.38819827
0.02	8.003522309	0.09	8.071240479	0.7	10.44298068	1.4	13.28865635	2.1	15.68414547	2.8	17.77248319	3.5	19.64478197

(Table continued)

TABLE II. *(Continued)*

h	Δ	h	Δ	h	Δ	h	Δ	h	Δ	h	Δ	h	Δ
0.03	8.007936951	0.1	8.087743676	0.8	10.88132504	1.5	13.65467247	2.2	15.99861037	2.9	18.05161545	3.6	19.89810453
0.04	8.014123318	0.2	8.333809063	0.9	11.30951572	1.6	14.01196194	2.3	16.30723744	3	18.32658527	3.7	20.14828534
0.05	8.022076090	0.3	8.689514097	1	11.72674009	1.7	14.36103169	2.4	16.61032468	3.1	18.59756906	3.8	20.39543679
0.06	8.031784032	0.4	9.105309717	1.1	12.13291167	1.8	14.70235789	2.5	16.90814740	3.2	18.86473149	3.9	20.63966483
0.07	8.043230095	0.5	9.547461271	1.2	12.52830852	1.9	15.03638379	2.6	17.20096028	3.3	19.12822650	4	20.88106951
							$S=6,\ J=2$						
0.1	8.203569714	0.7	12.20603873	1.3	15.49897496	1.9	18.19885941	2.5	20.54264637	3.1	22.64287866	3.7	24.56293047
0.2	8.749805252	0.8	12.81398438	1.4	15.98120006	2	18.61026177	2.6	20.90747748	3.2	22.97411099	3.8	24.86844381
0.3	9.455349474	0.9	13.39455794	1.5	16.44906143	2.1	19.01264899	2.7	21.26599112	3.3	23.30060162	3.9	25.17022884
0.4	10.18687108	1	13.95086879	1.6	16.90376973	2.2	19.40659215	2.8	21.61850638	3.4	23.62254953	4	25.46841936
0.5	10.89444030	1.1	14.48558849	1.7	17.34637701	2.3	19.79260451	2.9	21.96531626	3.5	23.94014012		
0.6	11.56726809	1.2	15.00098332	1.8	17.77780355	2.4	20.17114932	3	22.30669063	3.6	24.25354647		
							$S=8,\ J=2$						
0.01	10.00219865	0.05	10.05662485	0.5	13.24020821	0.9	16.04886720	1.3	18.42319871	1.7	20.51454711	2.1	22.40555577
0.02	10.00888017	0.2	10.83871352	0.6	13.99481542	1	16.67564783	1.4	18.96857094	1.8	21.00376124	2.2	22.85321150
0.03	10.02014469	0.3	11.62834664	0.7	14.71204219	1.1	17.27871723	1.5	19.49801146	1.9	21.48149240		
0.04	10.03605291	0.4	12.44740724	0.8	15.39546403	1.2	17.86053854	1.6	20.01296530	2	21.94852448		